

Electric dipole polarizabilities of Rydberg states of alkali atoms

V. A. Yerokhin,^{1,2} S. Y. Buhmann,^{3,4} S. Fritzsche,^{5,6} and A. Surzhykov^{1,7}

¹Physikalisch-Technische Bundesanstalt, D-38116 Braunschweig, Germany

²Center for Advanced Studies, Peter the Great St. Petersburg Polytechnic University, 195251 St. Petersburg, Russia

³Physikalisches Institut, Albert-Ludwigs Universität Freiburg, D-79104 Freiburg, Germany

⁴Freiburg Institute for Advanced Studies, Albert-Ludwigs Universität Freiburg, D-79104 Freiburg, Germany

⁵Helmholtz-Institut Jena, D-07743 Jena, Germany

⁶Theoretisch-Physikalisches Institut, Friedrich-Schiller-Universität Jena, D-07743 Jena, Germany

⁷Technische Universität Braunschweig, D-38106 Braunschweig, Germany

Calculations of the static electric-dipole scalar and tensor polarizabilities are presented for two alkali atoms, Rb and Cs, for the nS , $nP_{1/2, 3/2}$, and $nD_{3/2, 5/2}$ states with large principal quantum numbers up to $n = 50$. The calculations are performed within an effective one-electron approximation, based on the Dirac-Fock Hamiltonian with a semi-empirical core-polarization potential. The obtained results are compared with those from a simpler semi-empirical approach and with available experimental data.

I. INTRODUCTION

The term Rydberg atom refers to an atom with one (or several) valence electron(s) in a state with a large principal quantum number n . Such states are characterized by relatively long life time and huge polarizabilities ($\sim n^7$), which result in very large responses to electric and magnetic fields. Such exaggerated properties lead to strong, tunable interactions among the atoms, which have applications in various fields of physics. One of the prominent examples is the effect known as the Rydberg excitation blockade [1, 2]. In this effect, the excitation of more than one Rydberg atom within a blockade volume is suppressed, since such excited states are shifted out of resonance with a narrow-band excitation laser by the interaction between the Rydberg atoms.

The blockade effect relies on the energy level shift that one Rydberg atom experiences in a close proximity to another. Similar level shifts arise also when a Rydberg atom is brought into the vicinity of a macroscopic body or surface. With the constantly increasing experimental abilities to trap and manipulate atoms close to macroscopic bodies, the effects of the atom-surface interactions of the van der Waals [3] and Casimir-Polder [4] type have become a subject of great interest. When compared to atoms in their ground or lowest excited states, the Rydberg atoms exhibit various peculiarities of the atom-surface interactions, such as effects from the electric quadrupole and higher multipole moments [5], non-perturbative energy shifts, and surface-induced state mixing [6].

Theoretical description of the dynamics of Rydberg atoms in complex environments as well as their interactions with surfaces can be parameterized in terms of several basic atomic properties, such as transition energies, dipole matrix elements and atomic polarizabilities. Their integral convolution with the Green's tensor of the electric field in the macroscopic environment provides [7, 8] expressions for physical observables (decay rates, environment-induced energy shift, etc.). A classical example is the Casimir-Polder interaction potential be-

tween an atom and a perfectly conducting wall,

$$U(z) = -\frac{\hbar}{(4\pi)^2 \varepsilon_0 z^3} \int_0^\infty d\omega \alpha_0(i\omega) \times \left[1 + 2\frac{\omega z}{c} + 2\left(\frac{\omega z}{c}\right)^2 \right] e^{-2\omega z/c}, \quad (1)$$

which requires the detailed knowledge of the dynamic dipole polarizability of the atom at imaginary energies $\alpha_0(i\omega)$.

In order to describe the interaction of the Rydberg atoms with a complex macroscopic environment, first of all, we require a robust numerical approach for calculating energy levels, dipole transition matrix elements and atomic polarizabilities. In the present paper, we develop such a numerical approach and apply it for computations of static electric polarizabilities, for which numerous experimental and theoretical results are available in the literature. A comparison of the results obtained by different theoretical approaches and the experimental data helps us to establish the level of accuracy of our treatment.

In the present work we consider the alkali atoms, with a single highly excited valence electron beyond a closed-shell core. Their spectrum resembles that of the hydrogen atom and can be well described by effective one-electron approximations. The approach used in this work is based on the Dirac-Fock Hamiltonian with a semi-empirical core polarization potential. By using a finite basis set representation of the functional space, we obtain the spectrum of the eigenvalues and eigenfunctions the Hamiltonian, which allows us to compute various atomic properties, in particular, polarizabilities. By comparing the results obtained by this method with those from a simpler semi-empirical approach (the so-called Coulomb approximation), we get an idea about the uncertainty of our treatment.

The remaining paper is organized as follows. In Sec. II we give the outline of the theory of the atomic polarizabilities. The Dirac-Fock-Core-Polarization approach is discussed in Sec. III. In Sec. IV we describe the semi-empirical Coulomb approximation approach to the evaluation of the atomic polarizabilities. Our results are presented and discussed in Sec. V. The paper ends with a short conclusion in Sec. VI.

II. ATOMIC POLARIZABILITIES

A. General theory

Electric polarizabilities most naturally appear when considering energy shifts of atomic levels induced by the interaction with a classical external electric field (Stark effect). In the nonrelativistic theory, the interaction with a static electric field \mathbf{E} is given by the operator

$$H = -\boldsymbol{\mu} \cdot \mathbf{E}, \quad (2)$$

where $\boldsymbol{\mu} = -e \sum_i \mathbf{r}_i$ is the electric dipole operator, e is the electric charge and \mathbf{r}_i is the position vector of the i th electron. Due to symmetry arguments, the first-order expectation value of H on any atomic state vanishes but the higher-order perturbation contributions survive. We are presently interested in the second-order Stark effect, caused by the effective interaction of the form

$$H_{2\text{Stark}} = \boldsymbol{\mu} \cdot \mathbf{E} \frac{1}{E_0 - H_0} \boldsymbol{\mu} \cdot \mathbf{E}, \quad (3)$$

where H_0 is the Hamiltonian of the atom in the absence of the electric field and E_0 denotes its eigenvalue. The operator (3) can be conveniently represented as a sum of the scalar and the tensor parts,

$$H_{2\text{Stark}} = H_0 + H_2 \\ = \sum_{K=0,2} \sum_{Q=-K}^K (-1)^Q \left\{ \boldsymbol{\mu} \frac{1}{E_0 - H_0} \boldsymbol{\mu} \right\}_Q^K \{ \mathbf{E} \mathbf{E} \}_{-Q}^K, \quad (4)$$

where H_0 and H_2 correspond to $K = 0$ and $K = 2$, respectively, and $\{ \dots \}_Q^K$ denotes the tensor product of two vectors,

$$\{ \mathbf{L} \mathbf{M} \}_Q^K = \sum_{qq'} C_{1q,1q'}^{KQ} \mathbf{L}_q \mathbf{M}_{q'}.$$

The static electric-dipole scalar and tensor polarizabilities (α_0 and α_2 , respectively) are defined [9] from the matrix elements of H_0 and H_2 between the $M = J$ (so-called ‘‘stretched’’) states,

$$\langle JJ | H_0 | JJ \rangle = -\frac{1}{2} \alpha_0(J) E^2, \quad (5)$$

$$\langle JJ | H_2 | JJ \rangle = -\frac{1}{4} \alpha_2(J) (3E_z^2 - E^2). \quad (6)$$

The quadratic Stark shift of the energy level (J, M) then takes the form [9]

$$\Delta E = -\frac{1}{2} \alpha_0(J) E^2 - \frac{1}{4} \alpha_2(J) \frac{3M^2 - J(J+1)}{J(2J-1)} (3E_z^2 - E^2), \quad (7)$$

The polarizabilities can be expressed in terms of the reduced matrix elements of the operator $\boldsymbol{\mu}$ as follows [9]

$$\alpha_0(J) = -\frac{2}{3(2J+1)} \sum_n (-1)^{J_n - J} \frac{\langle 0J || \boldsymbol{\mu} || nJ_n \rangle \langle nJ_n || \boldsymbol{\mu} || 0J \rangle}{E_0 - E_n}, \quad (8)$$

$$\alpha_2(J) = (-1)^{2J+1} \sqrt{\frac{40J(2J-1)}{3(J+1)(2J+1)(2J+3)}} \\ \times \sum_n \left\{ \begin{matrix} 1 & 1 & 2 \\ J & J & J_n \end{matrix} \right\} \frac{\langle 0J || \boldsymbol{\mu} || nJ_n \rangle \langle nJ_n || \boldsymbol{\mu} || 0J \rangle}{E_0 - E_n}, \quad (9)$$

where the sum over n implies the summation over the complete spectrum of intermediate states of the atomic Hamiltonian. It follows from the above expression that α_2 vanishes for $J = 0$ and $1/2$.

B. Effective one-electron approximation

In the present investigation we are interested in the highly excited Rydberg states of alkali atoms. Such systems can be effectively described within an effective one-electron model, in which the valence electron interacts with the nuclear charge and the core. The direct contribution from the core polarizability is small as compared to the valence-electron polarizability (because of the n^7 scaling) and can be neglected. The indirect core-polarizability contribution, however, is sizeable (as it modifies the valence and intermediate-state electron energies and wave functions) and accounted for by the core polarization potential in the Hamiltonian.

In an effective one-electron approximation, the electric-dipole polarizabilities of a state v can be evaluated as

$$\alpha_0(v) = \frac{2}{3(2j_v + 1)} \sum_n \frac{[C_1(\kappa_v, \kappa_n) R_{vn}^{(1)}]^2}{\varepsilon_n - \varepsilon_v}, \quad (10)$$

$$\alpha_2(v) = \sqrt{\frac{40j_v(2j_v-1)}{3(j_v+1)(2j_v+1)(2j_v+3)}} \\ \times \sum_n (-1)^{j_v + j_n} \left\{ \begin{matrix} 1 & 1 & 2 \\ j_v & j_v & j_n \end{matrix} \right\} \frac{[C_1(\kappa_v, \kappa_n) R_{vn}^{(1)}]^2}{\varepsilon_n - \varepsilon_v}, \quad (11)$$

where the sum over n runs over the complete spectrum of virtual excited states, ε is the energy of the corresponding state, κ denotes the Dirac angular momentum-parity quantum number, j is the total angular momentum quantum number, $j = |\kappa| - 1/2$. The radial integrals are given by

$$R_{vn}^{(L)} = \int_0^\infty dr r^{2+L} W_{vn}(r), \quad (12)$$

where

$$W_{vn}(r) = g_v(r) g_n(r) + f_v(r) f_n(r), \quad (13)$$

where $g(r)$ and $f(r)$ are the upper and the lower radial components of the Dirac wave function, respectively. The angular coefficients are given by

$$C_J(\kappa_a, \kappa_b) = (a || C^{(J)} || b) = (-1)^J \sqrt{2j_a + 1} C_{j_a^{1/2}, J 0}^{j_b^{1/2}} \\ \times \Pi(l_a, l_b, J), \quad (14)$$

where $C^{(J)}$ denotes the normalized spherical harmonics, the symbol $\Pi(l_1, l_2, l_3)$ is unity if $l_1 + l_2 + l_3$ is even, and zero otherwise, and l is the orbital angular momentum quantum number, $l = |\kappa + 1/2| - 1/2$.

In the present work, we calculate the polarizabilities α_0 and α_2 of highly excited states of alkali atoms within the effective one-electron approaches, which are discussed in the next two sections.

III. DIRAC-FOCK-CORE-POLARIZATION HAMILTONIAN

The radial Dirac-Fock equation with a core-polarization (CP) potential (termed hereafter as the DFCP equation) is given by

$$h_{\text{DFCP}} \phi_a(r) = \varepsilon_a \phi_a(r), \quad (15)$$

where h_{DFCP} is the Hamiltonian, $\phi_a(r)$ is a two-component radial wave function

$$\phi_a(r) = \begin{pmatrix} g_a(r) \\ f_a(r) \end{pmatrix},$$

and ε_a is the energy eigenvalue. The DFCP Hamiltonian is given by

$$h_{\text{DFCP}} = \begin{pmatrix} m + V(r) & -\frac{1}{r} \frac{d}{dr} r + \frac{\kappa_a}{r} \\ \frac{1}{r} \frac{d}{dr} r + \frac{\kappa_a}{r} & -m + V(r) \end{pmatrix}. \quad (16)$$

The potential $V(r)$ in the above equation is

$$V(r) = V_{\text{nuc}}(r) + V_{\text{DF}}(r) + V_{\text{CP}}(r), \quad (17)$$

where V_{nuc} is the binding nuclear potential, V_{DF} is the frozen-core Dirac-Fock potential and V_{CP} is the core-polarization potential. The Dirac-Fock potential for the case of the interaction with a closed shell is defined by its matrix elements ($a \notin c$),

$$\langle a | V_{\text{DF}} | a \rangle = \alpha \sum_{c \in \text{core}} \left[(2j_c + 1) R_0(acac) - \frac{1}{2j_a + 1} \sum_L [C_L(\kappa_a, \kappa_c)]^2 R_L(acca) \right], \quad (18)$$

where index c runs over all different core states, and R_L are the Slater integrals

$$R_L(abcd) = \int_0^\infty dr_1 dr_2 (r_1 r_2)^2 \frac{r_{\leq}^L}{r_{>}^{L+1}} W_{ac}(r_1) W_{bd}(r_2). \quad (19)$$

The semi-empirical CP potential partly accounts for the second- and higher-order interaction of the valence electron with the core. It is given by (see, e.g., Ref. [10, 11])

$$V_{\text{CP}}(r) = -\frac{\alpha_c}{2r^4} (1 - e^{-r^6/\rho_\kappa^6}), \quad (20)$$

where α_c is the static dipole polarizability of the core and ρ_κ is the radial cutoff parameter, to be adjusted empirically.

In the present work we are interested in the complete energy spectrum of h_{DFCP} and the corresponding set of eigenstates. We obtain these numerically in several steps. In the first step, we compute the core wave functions c by solving the standard Dirac-Fock equation for the (closed-shell) core. In the second step, we solve the DFCP equation with help of the finite basis set constructed with B splines, using the core wave functions obtained in the first step for the evaluation of the matrix elements of the DF potential. The finite basis set method provides us with (a discrete representation of) the complete spectrum of the DFCP equation. In the third step, we fix the empirical value of the CP cutoff parameter ρ_κ (one for each κ) by matching the experimental energies in the high- n region.

The solution of the Dirac equation with a finite basis constructed with B splines have been first introduced in Ref. [12]. In present work, we solve the DFCP equation with a modification of the B -splines approach, namely, the Dual Kinetic Balance (DKB) method [13]. Within this method, the two-component solutions of Eq. (15) are approximated by an expansion over the finite basis of $2N$ functions u_n ,

$$\phi_a = \sum_{n=1}^{2N} c_n u_n = \sum_{i=1}^N c_i \begin{pmatrix} B_i(r) \\ \frac{1}{2m} \left(\frac{d}{dr} + \frac{\kappa_a}{r} \right) B_i(r) \end{pmatrix} + \sum_{i=1}^N c_{i+N} \begin{pmatrix} \frac{1}{2m} \left(\frac{d}{dr} - \frac{\kappa_a}{r} \right) B_i(r) \\ B_i(r) \end{pmatrix}, \quad (21)$$

where $\{B_i(r)\}_{i=1}^N$ is the set of B splines [14] on the interval $r = 0 \dots R_{\text{max}}$, where R_{max} is the cavity radius (chosen to be sufficiently large in order to have no influence on the calculated properties of the atom). We note that the ansatz (21) assumes that the potential in the Dirac equation is regular at $r \rightarrow 0$. This means that it can be used for solving the Dirac equation for an extended-nucleus potential, but *not* for the point-nucleus Coulomb potential.

The expansion (21) and the standard action principle lead to a generalized eigenvalue problem for the coefficients c_k ,

$$[\langle u_i | h_{\text{DFCP}} | u_k \rangle + \langle u_k | h_{\text{DFCP}} | u_i \rangle] c_k = 2E \langle u_i | u_k \rangle c_k, \quad (22)$$

where the summation over repeated indices is implied and $i, k = 1 \dots 2N$. The equation (22) is solved by the standard methods of linear algebra. Using the boundary conditions $\phi(0) = \phi(R) = 0$, we obtain a finite basis representation of the complete spectrum of the DFCP equation.

In the present work we are interested in highly excited Rydberg states of an atom, with the principal quantum number up to $n = 50$. It is nontrivial task to obtain an accurate representation of such highly excited states by a finite basis set method. In the original studies [12, 13] only the first few excited states were accurately reproduced. In the present work, we searched for a way to increase the number of bound states in the pseudospectrum. We found that the number of bound

states depends, most pronounced, on the cavity radius R and, less so, on the radial grid and the number of basis functions. In our calculations for Rb atom, we used the cavity radius of about $R = 4000\text{-}5000$ a.u. and the radial grid that is equidistant $r \sim t$ within the nucleus and polynomial $r \sim t^4$ outside of the nucleus (where t denotes the equidistant grid). With the basis set of $N = 150 - 250$ B splines, we obtained a pseudospectrum with typically 60-70 bound states. We checked that, for the standard frozen-core Dirac-Fock potential, our results for the energies of the valence excited states agree very well with those obtained by the direct solution of the Dirac-Fock equation [15].

After reproducing the Dirac-Fock energies, we included the CP potential. For the core polarizability α_c we used the calculated results from the literature [16]. The cutoff parameter ρ_κ was adjusted empirically to match the experimental energies of nlj Rydberg states for high n . More specifically, for each angular momentum quantum number κ , we chose the value of ρ_κ that minimized the deviation of the DFCP energies from the experimental energies (as given by Eq. (23)) for the states with n from 20 to 50.

After we obtained the DFCP pseudospectrum, it is relatively straightforward to compute the α_0 and α_2 polarizabilities according to Eqs. (10) and (11). We would like to stress that in the DFCP approach, we take into account the complete spectrum of the DFCP equation, both the discrete and the continuum parts. The contribution of the continuum part of the spectrum was found to be rather small, which justifies the usage of the so-called ‘‘sum-over-states’’ method for calculating the atomic polarizabilities [17, 18].

IV. COULOMB APPROXIMATION

A. Quantum defect energies

The term ‘‘quantum defect’’ was introduced nearly a century ago by Schrödinger [19] (see Ref. [20] for a historical account). Since then the concept of the quantum defects was extensively used in the atomic physics, mostly (but not only) for the description of energy levels of Rydberg atoms.

The quantum defect approach suggests the parametrization of the energy levels of the valence-excited Rydberg states of alkali atoms in the form similar to that of the hydrogen atom,

$$E(n\kappa) \equiv \varepsilon(n\kappa) - m = -\frac{m_r \alpha^2}{2n^{*2}}, \quad (23)$$

where m_r is the reduced mass and n^* is the effective (fractional) principal quantum number which replaces the true (integer) principal quantum number n in the nonrelativistic hydrogen theory. The effective principal quantum number n^* is usually parameterized in terms of the quantum defect parameters $\delta_i \equiv \delta_i(\kappa)$ as follows

$$n^* = n - \sum_{i=0}^{\infty} \frac{\delta_{2i}}{(n - \delta_0)^{2i}}, \quad (24)$$

In practice, the expansion over i is terminated after a few first terms (usually, two).

The quantum defect parameters can be calculated by *ab initio* methods or, alternatively, extracted from experimental data. It should be noted that for high Rydberg states (typically, $n > 30$), the experimental data follow the parametrization (23)-(24) with a very high accuracy. For the two atoms considered here, Rb and Cs, the Rydberg spectra are extensively studied experimentally and highly accurate results for the quantum defect parameters are available. The literature values of quantum defect expansion coefficients used in this paper for Rb and Cs are collected in Table I.

B. Polarizabilities

It was demonstrated long ago [21] that the wave functions of excited atomic states at large distances from the nucleus can be effectively approximated by the modified Coulomb solutions with fractional principal quantum numbers that are obtained from the quantum defect energies (23). This simple semi-empirical approach (often referred to as the Coulomb Approximation, CA) allows one to evaluate various transition integrals, providing that their dominant contribution originates from large radial distances. The CA method was successively applied for calculating atomic polarizabilities of alkali atoms [22, 23] and was shown to yield results in a remarkably good (for such a simple approximation) agreement with experimental data. In the present work, we perform calculations of polarizabilities by the CA method and compare the results with those obtained with the more elaborated DFCP approach, in order to get an idea about the uncertainties of the theoretical treatment.

In the CA method, we assume the energies of the bound state of interest to be given by Eq. (23), with the quantum defect parameters determined from the experimental data. We now are looking for a solution of the Schrödinger equation that has a fractional principal quantum number n^* and is regular at $r \rightarrow \infty$. Naturally, since the corresponding energy is not the eigenvalue of the Schrödinger-Coulomb Hamiltonian, such a solution will diverge at $r \rightarrow 0$; but it will be of no importance for us since we are interested only in the large- r region. The exact solution of the Schrödinger equation with the Coulomb potential regular at $r \rightarrow \infty$ can be written as

$$G_{n^*l}(r) = (-1)^l n^* \Gamma[n^* + l - 1] \times \sqrt{\frac{\Gamma[n^* - l]}{\Gamma[n^* + l + 1]}} W_{n^*, l+1/2}(2r/n^*), \quad (25)$$

where the $W(x)$ is the Whittaker function, l is the orbital angular momenta, and n^* is the effective principal quantum number, as obtained from Eq. (24). It can be explicitly checked that for integer values of $n^* = n$, the function $G_{nl}(r)$ coincides with the well known nonrelativistic bound-state wave function.

In order to compute the radial integrals required for α_0 and α_2 , we made the replacement

$$R_{ab}^{(L)} \rightarrow \tilde{R}_{ab}^{(L)} = \int_{r_{\min}}^{\infty} dr r^L G_{n_a^* l_a}(r) G_{n_b^* l_b}(r), \quad (26)$$

where r_{\min} is a small radial cutoff parameter.

Following [21], we compute the Whittaker W function by its asymptotic expansion

$$W_{n^*, l+1/2}(2r/n^*) = e^{-r/n^*} \left(\frac{2r}{n^*} \right)^{n^*} \left[1 + \sum_{t=1}^{\infty} \frac{a_t}{r^k} \right] \quad (27)$$

with the expansion coefficients a_t obtained by the recurrence relation

$$\begin{aligned} a_t &= a_{t-1} \frac{n^*}{2t} [l(l+1) - (n^* - t)(n^* - t + 1)], \quad (28) \\ a_1 &= \frac{n^*}{2} [l(l+1) - n^*(n^* - 1)]. \quad (29) \end{aligned}$$

Based on our calculations we found that summation over t in Eq. (27) can be truncated at about $t_{\max} = n^* + 1$ without losses of accuracy in the evaluation of the radial integrals.

The integration in Eq. (26) was performed numerically by employing the Gauss–Legendre quadratures. Following Ref. [21], we defined the lower bound of the radial integration in Eq. (26) as $r_{\min} = s n_a n_b / (n_a + n_b)$ with $s \approx 1/100$. We have checked that the final results do not depend on the particular choice of the parameter s .

The sum over n in Eqs. (10) and (11) is performed by explicitly summing over the virtual excited bound states (the so-called “sum-over-states” method). The continuum part of the spectrum yields a very small contribution to polarizabilities and was neglected. The summation over n is extended until the convergence is reached (typically, about 20-30 virtual excited states are included).

V. RESULTS AND DISCUSSION

We start our discussion by analysing the energy values delivered by the DFCP method. Our numerical results for energy levels of Rb and Cs are presented in Table II, in comparison with the values obtained from the quantum defect formula (23) and the experimental quantum defect parameters from Table I. We observe that the DFCP method reproduces the experimental energies very well, provided that the principal quantum number n is large enough, typically $n \geq 20$. For smaller n 's, the deviation of the DFCP energies from the experimental values gradually increases as n decreases. We therefore expect that the accuracy of the DFCP results for the polarizabilities will not depend on n for $n \geq 20$ and will gradually deteriorate as n is decreased from $n = 20$ downwards.

In order to estimate the uncertainty of our theoretical description of polarizabilities, we compare the results obtained by two different methods, the DFCP and the CA ones. We expect that both methods should become essentially equivalent in the high- n limit; for smaller n 's, however, some deviations are expected. The difference between the results will give us an idea about the error of the treatment.

The comparison is presented in Table III. We observe that for $n \geq 15$, both methods give results equivalent at a 1% level for all the states considered. For the lower- n states, the situation is somewhat different for Rb and Cs. For Rb, the

agreement between the two methods is very good for the S and P states, whereas for D states there are deviations on a few % level. For Cs, we observe larger deviations than for Rb, which however disappear in the high- n limit.

We now compare our DFCP values of polarizabilities with previous experimental and theoretical results available in the literature. The comparison for α_0 and α_2 in Rb and Cs is presented in Tables IV-VII. The complete tabulation of our DFCP results is given in Tables I-IV of Supplementary Material. Results are reported for the states with the principal quantum number n in the region $n = 8 - 50$ for Rb and $n = 9 - 50$ for Cs.

We observe that for the nS states, there is a very good agreement between different calculations and also between theoretical and experimental values. In particular, we note excellent agreement with high-precision experimental results by Walls *et al.* [24] for the $9S$ and $10S$ states of Rb and those by Wijngaarden *et al.* [25] for the $11S$, $12S$, and $13S$ states of Cs. Based on this comparison and on the fact that the DFCP approach works better with the increase of n , we estimate that the accuracy of our DFCP results for the nS states should be better than 1% for all n 's presented in the tables.

For the P states, there is no experimental data available. Based on the comparison presented in Table III, we estimate that the accuracy of our results should be on the 1% level for $n \geq 15$. For the D states, we observe that deviations from the experimental data are larger than for the S and P states, and that they decrease more slowly with increase of n . We estimate that the accuracy of our results for the D states should be on the 1% level for $n \geq 20$ and on the 2% level for $n \approx 15$. We note some discrepancies with the CA results by Wijngaarden [22] for the $10D$ and $11D$ states of Rb (including the overall sign in the case of α_0 and a factor-of-about-two difference for α_2), which probably are due to numerical instabilities for high n 's in Ref. [22].

Finally, we analyse the n dependence of the electric polarizabilities. In Figs. 1 and 2 we plot our results for the α_0 and α_2 polarizabilities, scaled by their leading n dependence factor, n^{-7} . We find that for the S states, the polarizability demonstrates the asymptotic large- n behaviour already at $n \approx 20$, whereas for the P and D states the asymptotic behaviour is generally not reached in the range of $n \leq 50$ considered in the present work.

It might be now interesting to address the question to which extent the relativistic treatment is necessary in describing highly excited Rydberg states. In the literature, the behaviour of the high- n electrons is often considered to be non-relativistic, or even quasi-classical. From Table II we can deduce that the relativistic effect of the fine-structure splitting of nP_J , nD_J , and even nF_J (in the case of Cs) energy levels is rather significant on the level of the calculational accuracy. Theoretical treatment of the atomic polarizabilities is known to be very sensitive to the (rather small) energy difference of the reference state and the nearest excited states of the opposite parity and, therefore, requires energy levels calculated with inclusion of relativistic effects. Contrary to that, the transition matrix elements appearing in the expressions for α_0 and α_2 are essentially non-relativistic for high n . This is

confirmed by good agreement observed between the DFPC and CA methods (we recall that in the CA method, the radial integrals are calculated nonrelativistically, whereas the DFPC approach is fully relativistic).

VI. CONCLUSION

In this paper we have presented our calculations of the static electric-dipole scalar and tensor polarizabilities of highly excited nS , nP_j , and nD_j states of Rb and Cs. The calculations are based on the Dirac-Fock Hamiltonian with a semi-empirical core-polarization potential. This approach provides us with a complete spectrum of the energies and wavefunctions of the effective one-particle Hamiltonian and allows us to compute various atomic properties, in particular, atomic polarizabilities. By comparison with the results obtained by different methods and with the experimental data, we estimate

the accuracy of the obtained polarizability values to be on a % level for sufficiently high values of the principal quantum number n . In our future investigations we plan to employ this method for computing dynamic atomic polarizabilities and transition matrix elements necessary for the theoretical description of the interaction of Rydberg atoms with a macroscopic environment.

Acknowledgement

V.A.Y. acknowledges support by the Russian Federation program for organizing and carrying out scientific investigations and by RFBR (grant No. 16-02-00538). S.Y.B. gratefully acknowledges support by the German Research Foundation (grants BU 1803/3-1 and and GRK 2079/1) and the Freiburg Institute for Advanced Studies.

-
- [1] A. Gaetan, Y. Miroshnychenko, T. Wilk, A. Chotia, M. Viteau, D. Comparat, P. Pillet, A. Browaeys, and P. Grangier, *Nature Physics* **5**, 115 (2009).
- [2] E. Urban, T. A. Johnson, T. Henage, L. Isenhower, D. Yavuz, T. Walker, and M. Saffman, *Nature Physics* **5**, 110 (2009).
- [3] J. Lennard-Jones, *Transactions of the Faraday Society* **28**, 333 (1932).
- [4] H. Casimir and D. Polder, *Phys. Rev.* **73**, 360 (1948).
- [5] J. A. Crosse, S. A. Ellingsen, K. Clements, S. Y. Buhmann, and S. Scheel, *Phys. Rev. A* **82**, 010901 (2010).
- [6] S. Ribeiro, S. Y. Buhmann, T. Stielow, and S. Scheel, *Europhys. Lett.* **110**, 51003 (2015).
- [7] G. Agarwal, *Phys. Rev. A* **11**, 243 (1975).
- [8] G. Agarwal, *Phys. Rev. A* **12**, 1987 (1975).
- [9] J. R. P. Angel and P. G. H. Sandars, *Proc. R. Soc. London, Ser. A* **305**, 125 (1968).
- [10] D. W. Norcross and M. J. Seaton, *J. Phys. B* **9**, 2983 (1976).
- [11] J. Mitroy and D. W. Norcross, *Phys. Rev. A* **37**, 3755 (1988).
- [12] W. R. Johnson, S. A. Blundell, and J. Sapirstein, *Phys. Rev. A* **37**, 307 (1988).
- [13] V. M. Shabaev, I. I. Tupitsyn, V. A. Yerokhin, G. Plunien, and G. Soff, *Phys. Rev. Lett.* **93**, 130405 (2004).
- [14] C. de Boor, *A practical guide to splines*, Springer, New York, 1978.
- [15] V. F. Bratzev, G. B. Deyneka, and I. I. Tupitsyn, *Izv. Akad. Nauk SSSR, Ser. Fiz.* **41**, 2655 (1977), [*Bull. Acad. Sci. USSR, Phys. Ser.* **41**, 173 (1977)].
- [16] W. R. Johnson, D. Kolb, and K.-N. Huang, *At. Data Nucl. Data Tables* **28**, 333 (1983).
- [17] J. Mitroy, M. S. Safronova, and C. W. Clark, *J. Phys. B* **43**, 202001 (2010).
- [18] M. S. Safronova and U. I. Safronova, *Phys. Rev. A* **83**, 052508 (2011).
- [19] E. Schrödinger, *Z. Phys.* **4**, 347 (1921).
- [20] A. R. P. Rau and M. Inokuti, *Am. J. Phys.* **65**, 221 (1997).
- [21] D. R. Bates and A. Damgaard, *Phil. Trans. R. Soc. London* **242**, 101 (1949).
- [22] W. V. Wijngaarden, *J. Quant. Spect. Rad. Transf.* **52**, 555 (1994).
- [23] W. V. Wijngaarden, *J. Quant. Spect. Rad. Transf.* **57**, 275 (1997).
- [24] J. Walls, J. Clarke, S. Cauchi, G. Karkas, H. Chen, and W. van Wijngaarden, *Eur. Phys. J. D* **14**, 9 (2001).
- [25] W. A. van Wijngaarden, E. A. Hessels, J. Li, and N. E. Rothery, *Phys. Rev. A* **49**, R2220 (1994).
- [26] M. Mack, F. Karlewski, H. Hattermann, S. Höckh, F. Jessen, D. Cano, and J. Fortágh, *Phys. Rev. A* **83**, 052515 (2011).
- [27] Wenhui Li, I. Mourachko, M. W. Noel, and T. F. Gallagher, *Phys. Rev. A* **67**, 052502 (2003).
- [28] J. Han, Y. Jamil, D. V. L. Norum, P. J. Tanner, and T. F. Gallagher, *Phys. Rev. A* **74**, 054502 (2006).
- [29] J. Deiglmayr, H. Herburger, H. Saßmannshausen, P. Jansen, H. Schmutz, and F. Merkt, *Phys. Rev. A* **93**, 013424 (2016).
- [30] C. J. Lorenzen and K. Niemax, *Phys. Scr.* **27**, 300 (1983).
- [31] K.-H. Weber and C. J. Sansonetti, *Phys. Rev. A* **35**, 4650 (1987).
- [32] M. S. O'Sullivan and B. P. Stoicheff, *Phys. Rev. A* **31**, 2718 (1985).
- [33] M. S. O'Sullivan and B. P. Stoicheff, *Phys. Rev. A* **33**, 1640 (1986).
- [34] W. Hogervorst and S. Svanberg, *Phys. Scr.* **12**, 67 (1975).
- [35] K. Fredriksson and S. Svanberg, *Z. Phys. A* **281**, 189 (1977).
- [36] J. Xia, J. Clarke, J. Li, and W. A. van Wijngaarden, *Phys. Rev. A* **56**, 5176 (1997).
- [37] J. Zhao, H. Zhang, Z. Feng, X. Zhu, L. Zhang, C. Li, and S. Jia, *J. Phys. Soc. Japan* **80**, 034303 (2011).
- [38] T. Lei, S. Gu, Z. Weng, and X. Zeng, *Z. Phys. A* **34**, 139 (1995).

TABLE I: Experimental quantum defect parameters for Rb and Cs.

	$n^2S_{1/2}$	$n^2P_{1/2}$	$n^2P_{3/2}$	$n^2D_{3/2}$	$n^2D_{5/2}$	$n^2F_{5/2}$	$n^2F_{7/2}$
Rb							
Ref.	[26, 27]	[27]	[27]	[26, 27]	[26, 27]	[28]	[28]
δ_0	3.131 180 6(10)	2.654 884 9(10)	2.641 673 7(10)	1.348 093(2)	1.346 464(2)	0.016 519 2(9)	0.016 543 7(7)
δ_2	0.178 6 (6)	0.290 0 (6)	0.295 0 (7)	-0.604 2 (13)	-0.595 0 (11)	-0.085 (9)	-0.086 (7)
Cs							
Ref.	[29]	[29]	[29]	[30]	[29]	[31]	
δ_0	4.049 353 2(4)	3.591 587 1(3)	3.559 067 6(3)	2.475 45 (2)	2.466 314 4(6)	0.033 414(1)	
δ_2	0.239 1 (5)	0.362 73 (16)	0.374 69 (14)	0.009 9 (40)	0.013 81 (15)	-0.198 674	
δ_4	0.06 (10)			-0.433 24	-0.392 (12)	0.289 53	
δ_6	11(7)			-0.965 55	-1.9(3)	-0.260 1	
δ_8	-209(150)			-16.946 4			

TABLE II: Energies of the valence-excited states of Rb and Cs, for the infinitely heavy nucleus, in a.u. For each n , the upper line displays the calculated DFCP energies, whereas the lower line presents the experimental energies as obtained from Eq. (23) with the quantum defect parameters taken from Table I. The parameters of the DFCP potential are [16] $\alpha_c(\text{Rb}) = 9.076 a_0^3$, $\alpha_c(\text{Cs}) = 15.81 a_0^3$ and ρ_κ as specified in the table.

	$n^2S_{1/2}$	$n^2P_{1/2}$	$n^2P_{3/2}$	$n^2D_{3/2}$	$n^2D_{5/2}$	$n^2F_{5/2}$	$n^2F_{7/2}$
Rb							
ρ_κ	2.433	2.358	2.354	2.799	2.817	2.817	2.817
$n = 20$	0.001 757 247 0.001 757 248	0.001 662 127 0.001 662 126	0.001 659 599 0.001 659 600	0.001 436 956 0.001 436 953	0.001 436 707 0.001 436 706	0.001 252 040 0.001 252 041	0.001 252 045 0.001 252 044
$n = 30$	0.000 692 597 0.000 692 597	0.000 668 687 0.000 668 687	0.000 668 042 0.000 668 042	0.000 609 027 0.000 609 033	0.000 608 958 0.000 608 964	0.000 556 165 0.000 556 164	0.000 556 166 0.000 556 165
$n = 40$	0.000 367 837 0.000 367 836	0.000 358 515 0.000 358 515	0.000 358 262 0.000 358 261	0.000 334 669 0.000 334 672	0.000 334 640 0.000 334 644	0.000 312 758 0.000 312 757	0.000 312 758 0.000 312 758
$n = 50$	0.000 227 616 0.000 227 616	0.000 223 059 0.000 223 060	0.000 222 934 0.000 222 936	0.000 211 233 0.000 211 235	0.000 211 219 0.000 211 221	0.000 200 131 0.000 200 132	0.000 200 131 0.000 200 132
Cs							
ρ_κ	2.782	2.666	2.677	3.142	3.181	2.94	2.94
$n = 20$	0.001 965 468 0.001 965 462	0.001 857 419 0.001 857 412	0.001 850 080 0.001 850 079	0.001 628 123 0.001 628 088	0.001 626 428 0.001 626 393	0.001 254 125 0.001 254 125	0.001 254 163 0.001 254 125
$n = 30$	0.000 742 480 0.000 742 481	0.000 716 972 0.000 716 973	0.000 715 209 0.000 715 211	0.000 659 978 0.000 659 979	0.000 659 539 0.000 659 541	0.000 556 787 0.000 556 787	0.000 556 798 0.000 556 787
$n = 40$	0.000 386 866 0.000 386 866	0.000 377 201 0.000 377 201	0.000 376 528 0.000 376 528	0.000 355 089 0.000 355 091	0.000 354 916 0.000 354 918	0.000 313 021 0.000 313 021	0.000 313 025 0.000 313 021
$n = 50$	0.000 236 804 0.000 236 804	0.000 232 156 0.000 232 156	0.000 231 831 0.000 231 831	0.000 221 377 0.000 221 378	0.000 221 291 0.000 221 293	0.000 200 266 0.000 200 267	0.000 200 268 0.000 200 267

TABLE III: Comparison of results obtained by two different methods, DFCP and CA, for the static dipole polarizabilities α_0 of neutral Rb and Cs atoms, in a_0^3 ($a_0 \approx 0.052918$ nm is the Bohr radius). For each principal quantum number n , predictions of the DFCP method are given in the upper line and those of the CA method, in the lower line. $X[b]$ means $X \times 10^b$.

n	n^2S	$n^2P_{1/2}$	$n^2P_{3/2}$	$n^2D_{3/2}$	$n^2D_{5/2}$
Rb					
8	0.133 [6] 0.132 [6]	0.363 [6] 0.364 [6]	0.395 [6] 0.395 [6]	0.909 [6] 0.937 [6]	0.877 [6] 0.905 [7]
10	0.109 [7] 0.109 [7]	0.328 [7] 0.327 [7]	0.357 [7] 0.356 [7]	0.479 [7] 0.490 [7]	0.458 [7] 0.469 [7]
12	0.528 [7] 0.527 [7]	0.171 [8] 0.171 [8]	0.187 [8] 0.186 [8]	0.178 [8] 0.181 [8]	0.169 [8] 0.172 [8]
15	0.321 [8] 0.321 [8]	0.115 [9] 0.115 [9]	0.126 [9] 0.126 [9]	0.858 [8] 0.867 [8]	0.803 [8] 0.812 [8]
20	0.289 [9] 0.289 [9]	0.118 [10] 0.118 [10]	0.130 [10] 0.130 [10]	0.629 [9] 0.631 [9]	0.580 [9] 0.582 [9]
30	0.555 [10] 0.554 [10]	0.269 [11] 0.269 [11]	0.297 [11] 0.297 [11]	0.101 [11] 0.101 [11]	0.909 [10] 0.905 [10]
Cs					
9	0.154 [6] 0.152 [6]	0.105 [7] 0.102 [7]	0.136 [7] 0.131 [7]	-0.146 [7] -0.140 [7]	-0.185 [7] -0.178 [7]
10	0.477 [6] 0.474 [6]	0.356 [7] 0.350 [7]	0.463 [7] 0.452 [7]	-0.436 [7] -0.423 [7]	-0.548 [7] -0.531 [7]
12	0.286 [7] 0.286 [7]	0.246 [8] 0.243 [8]	0.321 [8] 0.316 [8]	-0.254 [8] -0.250 [8]	-0.315 [8] -0.310 [8]
15	0.211 [8] 0.211 [8]	0.210 [9] 0.209 [9]	0.275 [9] 0.273 [9]	-0.188 [9] -0.187 [9]	-0.231 [9] -0.230 [9]
20	0.226 [9] 0.226 [9]	0.267 [10] 0.266 [10]	0.350 [10] 0.349 [10]	-0.212 [10] -0.211 [10]	-0.258 [10] -0.257 [10]
30	0.511 [10] 0.511 [10]	0.740 [11] 0.740 [11]	0.972 [11] 0.971 [11]	-0.526 [11] -0.527 [11]	-0.636 [11] -0.636 [11]

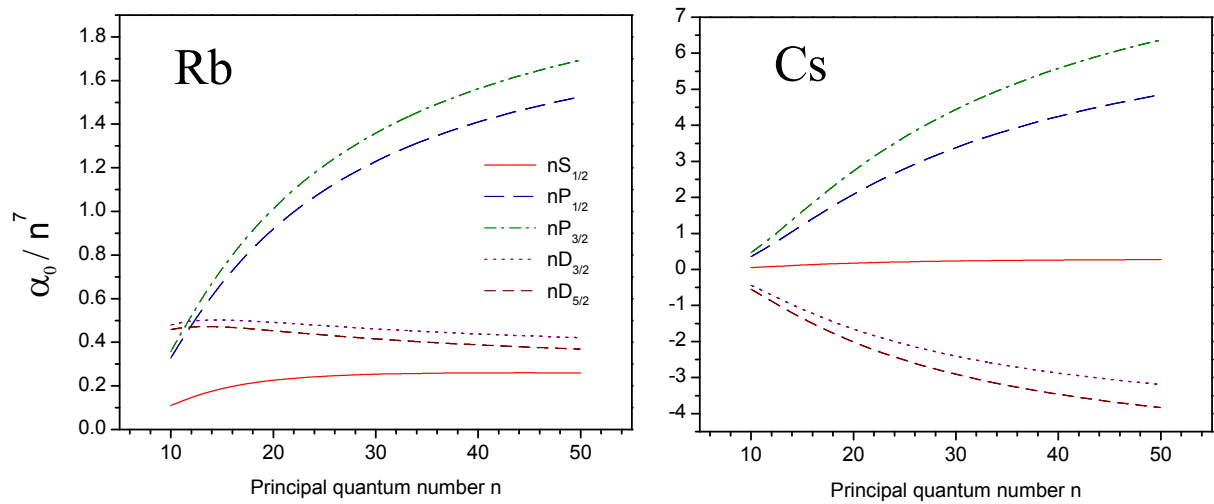


FIG. 1: (Color online) Electric dipole polarizabilities α_0 scaled by the prefactor of n^{-7} , as a function of the principal quantum number n , for Rb (left graph) and Cs (right graph).

TABLE IV: Static electric-dipole scalar polarizabilities α_0 (in a_0^3) in Rb, a comparison with the previous experimental and theoretical results. The complete tabulation of the DFCP results is available in Table I of Supplementary Material. The notations are as follows: $X[b]$ means $X \times 10^b$; $X(a)[b]$ means $X \times 10^b$ with uncertainty a in the last digit of X ; “(th)” and “(exp)” refer to the theoretical and the experimental literature results, correspondingly.

n	n^2S	$n^2P_{1/2}$	$n^2P_{3/2}$	$n^2D_{3/2}$	$n^2D_{5/2}$	Ref.
8	0.133 [6]	0.363 [6]	0.395 [6]	0.909 [6]	0.877 [6]	
	0.132 [6]	0.360 [6]	0.391 [6]	0.936 [6]	0.904 [7]	[23] (th)
	0.133(1) [6]					[18] (th)
9				0.927(1) [6]	0.8949(6) [6]	[24] (exp)
	0.417 [6]	0.120 [7]	0.130 [7]	0.221 [7]	0.212 [7]	
	0.416 [6]	0.119 [7]	0.129 [7]	0.226 [7]	0.217 [7]	[23] (th)
	0.417(2) [6]					[18] (th)
10	0.4170(4) [6]					[24] (exp)
	0.109 [7]	0.328 [7]	0.357 [7]	0.479 [7]	0.458 [7]	
	0.110 [7]	0.326 [7]	0.355 [7]	-0.485 [7]	-0.514 [7]	[23] (th)
	0.1094(6) [7]					[18] (th)
11	0.10953(6) [7]					[24] (exp)
	0.252 [7]	0.787 [7]	0.859 [7]	0.956 [7]	0.909 [7]	
12	0.251 [7]	0.782 [7]	0.854 [7]	0.935 [7]	-0.999 [7]	[23] (th)
	0.528 [7]	0.171 [8]	0.187 [8]	0.178 [8]	0.169 [8]	
13	0.526 [7]	0.137 [8]	0.151 [8]			[23] (th)
	0.102 [8]	0.343 [8]	0.375 [8]	0.314 [8]	0.296 [8]	
15		0.346 [8]	0.370 [8]			[23] (th)
				0.314(1) [8]	0.283(2) [8]	[32, 33] (exp)
	0.321 [8]	0.115 [9]	0.126 [9]	0.858 [8]	0.803 [8]	
20	0.319(2) [8]			0.860(8) [8]	0.796(4) [8]	[32, 33] (exp)
	0.289 [9]	0.118 [10]	0.130 [10]	0.629 [9]	0.580 [9]	
25	0.2905(12) [9]			0.643(12) [9]	0.583(8) [9]	[32, 33] (exp)
	0.149 [10]	0.670 [10]	0.740 [10]	0.291 [10]	0.264 [10]	
30	0.151(2) [10]			0.297(12) [10]	0.265(4) [10]	[32, 33] (exp)
	0.555 [10]	0.269 [11]	0.297 [11]	0.101 [11]	0.909 [10]	
35	0.559(6) [10]			0.104(4) [11]	0.936(8) [10]	[32, 33] (exp)
	0.166 [11]	0.856 [11]	0.948 [11]	0.289 [11]	0.258 [11]	
40	0.169(1) [11]			0.297(8) [11]	0.253(8) [11]	[32, 33] (exp)
	0.425 [11]	0.231 [12]	0.256 [12]	0.718 [11]	0.636 [11]	
45	0.425(8) [11]			0.74(3) [11]	0.67(2) [11]	[32, 33] (exp)
	0.972 [11]	0.551 [12]	0.611 [12]	0.160 [12]	0.141 [12]	
50	1.00(4) [11]			0.169(8) [12]	0.153(8) [12]	[32, 33] (exp)
	0.203 [12]	0.119 [13]	0.132 [13]	0.329 [12]	0.288 [12]	
	0.203(1) [12]			0.341(12) [12]	0.289(16) [12]	[32, 33] (exp)

TABLE V: Static electric-dipole tensor polarizabilities α_2 (in a_0^5) in Rb, a comparison with the previous experimental and theoretical results. The complete tabulation of the DFCP results is available in Table II of Supplementary Material. Notations are as in Table IV.

n	$n^2 P_{3/2}$	$n^2 D_{3/2}$	$n^2 D_{5/2}$	Ref.
8	-0.513 [5]	0.113 [6]	0.223 [6]	
	-0.508 [5]	0.105 [6]	0.211 [6]	[23] (th)
		0.109(6) [6]	0.229(12) [6]	[34] (exp)
		0.1067(4) [6]	0.2086(4) [6]	[24] (exp)
9	-0.161 [6]	0.389 [6]	0.723 [6]	
	-0.160 [5]	0.373 [6]	0.701 [6]	[23] (th)
10	-0.427 [6]	0.107 [7]	0.194 [7]	
	-0.424 [6]	0.299 [7]	0.470 [7]	[23] (th)
11	-0.996 [6]	0.256 [7]	0.455 [7]	
	-0.974 [6]	0.633 [7]	0.998 [7]	[23] (th)
13	-0.414 [7]	0.110 [8]	0.191 [8]	
	-0.366 [7]	0.108(2) [8]	0.189(4) [8]	[33] (exp)
15	-0.134 [8]	0.361 [8]	0.620 [8]	
		0.354(8) [8]	0.607(8) [8]	[33] (exp)
20	-0.130 [9]	0.359 [9]	0.606 [9]	
		0.358(12) [9]	0.599(20) [9]	[33] (exp)
25	-0.710 [9]	0.200 [10]	0.335 [10]	
		0.201(8) [10]	0.326(4) [10]	[33] (exp)
30	-0.277 [10]	0.791 [10]	0.132 [11]	
		0.784(20) [10]	0.129(4) [11]	[33] (exp)
35	-0.865 [10]	0.249 [11]	0.415 [11]	
		0.249(8) [11]	0.418(8) [11]	[33] (exp)
40	-0.230 [11]	0.668 [11]	0.111 [12]	
		0.64(3) [11]	0.11(4) [12]	[33] (exp)
45	-0.541 [11]	0.158 [12]	0.263 [12]	
		0.157(12) [12]	0.257(12) [12]	[33] (exp)
50	-0.116 [12]	0.341 [12]	0.566 [12]	
		0.329(12) [12]	0.539(20) [12]	[33] (exp)

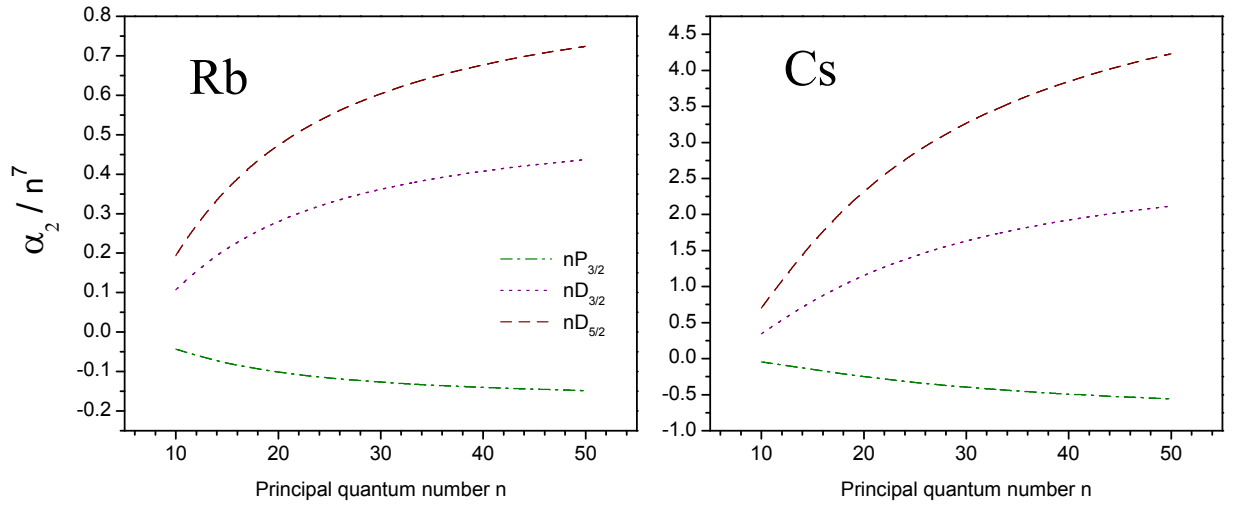


FIG. 2: (Color online) Electric tensor polarizabilities α_2 scaled by the prefactor of n^{-7} , as a function of the principal quantum number n , for Rb (left graph) and Cs (right graph).

TABLE VI: Static electric-dipole scalar polarizabilities α_0 (in a_0^3) in Cs, a comparison with the previous experimental and theoretical results. The complete tabulation of the DFCP results is available in Table III of Supplementary Material. Notations are as in Table IV.

n	n^2S	$n^2P_{1/2}$	$n^2P_{3/2}$	$n^2D_{3/2}$	$n^2D_{5/2}$	Ref.
9	0.154 [6]	0.105 [7]	0.136 [7]	-0.146 [7]	-0.185 [7]	
	0.153 [6]	0.102 [7]	0.131 [7]	-0.140 [7]	-0.177 [7]	[22] (th)
10				-0.14(1) [7]	-0.20(1) [7]	[35] (exp)
	0.477 [6]	0.356 [7]	0.463 [7]	-0.436 [7]	-0.548 [7]	
	0.475 [6]	0.349 [7]	0.451 [7]	-0.422 [7]	-0.530 [7]	[22] (th)
				-0.46(7) [7]	-0.54(5) [7]	[35] (exp)
				-0.4185(4) [7]	-0.5303(8) [7]	[36] (exp)
11	0.478(1) [6]					[25] (exp)
	0.125 [7]	0.100 [8]	0.131 [8]	-0.111 [8]	-0.139 [8]	
	0.124 [7]	0.099 [8]	0.128 [8]	-0.109 [8]	-0.136 [8]	[22] (th)
12				-0.1083(1) [8]	-0.1358(2) [8]	[36] (exp)
	0.1245(1) [7]					[25] (exp)
	0.286 [7]	0.246 [8]	0.321 [8]	-0.254 [8]	-0.315 [8]	
13	0.284 [7]	0.244 [8]	0.316 [8]	-0.251 [8]	-0.311 [8]	[22] (th)
				-0.2484(2) [8]	-0.3078(6) [8]	[36] (exp)
	0.2867(2) [7]					[25] (exp)
14	0.598 [7]	0.543 [8]	0.709 [8]	-0.530 [8]	-0.655 [8]	
	0.590 [7]	0.540 [8]	0.703 [8]	-0.522 [8]	-0.647 [8]	[22] (th)
				-0.5198(7) [8]	-0.643(1) [8]	[36] (exp)
15	0.5993(5) [7]					[25] (exp)
	0.116 [8]	0.110 [9]	0.144 [9]	-0.103 [9]	-0.127 [9]	
16	0.114 [8]	0.110 [9]	0.143 [8]			[22] (th)
	0.211 [8]	0.210 [9]	0.275 [9]	-0.188 [9]	-0.231 [9]	
17	0.206 [8]					[22] (th)
	0.365 [8]	0.378 [9]	0.496 [9]	-0.328 [9]	-0.403 [9]	
18	0.354 [8]					[22] (th)
	0.605 [8]	0.651 [9]	0.853 [9]	-0.550 [9]	-0.672 [9]	
19	0.577 [8]					[22] (th)
	0.355 [11]	0.573 [12]	0.753 [12]	-0.390 [12]	-0.469 [12]	
20				-0.45(2) [12]	-0.49(2) [12]	[37] (exp)
	0.215 [12]	0.379 [13]	0.498 [13]	-0.249 [13]	-0.300 [13]	
21				-0.206(6) [13]	-0.28(1) [13]	[37] (exp)

TABLE VII: Static electric-dipole tensor polarizabilities α_2 (in a_0^3) in Cs, a comparison with the previous experimental and theoretical results. The complete tabulation of the DFCP results is available in Table IV of Supplementary Material. Notations are as in Table IV.

n	$n^2 P_{3/2}$	$n^2 D_{3/2}$	$n^2 D_{5/2}$	Ref.
9	-0.138 [6]	0.121 [7]	0.245 [7]	[22] (th)
	-0.134 [6]	0.119 [7]	0.238 [7]	
10	-0.460 [6]	0.347 [7]	0.701 [7]	[22] (th)
	-0.449 [6]	0.341 [7]	0.685 [7]	[36] (exp)
		0.3401(4) [7]	0.682(2) [7]	
11	-0.127 [7]	0.860 [7]	0.174 [8]	[22] (th) [36] (exp)
	-0.125 [7]	0.852 [7]	0.171 [8]	
		0.847(1) [7]	0.1705(5) [8]	
12	-0.308 [7]	0.192 [8]	0.387 [8]	[22] (th)
	-0.305 [7]	0.191 [8]	0.383 [8]	
13	-0.673 [7]	0.393 [8]	0.792 [8]	[22] (th)
	-0.670 [7]	0.389 [8]	0.785 [8]	[36] (exp)
		0.3866(7) [8]	0.780(2) [8]	
14	-0.136 [8]	0.753 [8]	0.152 [9]	[22] (th)
	-0.136 [8]		0.149(8) [9]	[35] (exp)
15	-0.257 [8]	0.136 [9]	0.274 [9]	[35] (exp)
			0.28(2) [9]	
16	-0.460 [8]	0.235 [9]	0.474 [9]	[35] (exp)
			0.48(2) [9]	
17	-0.786 [8]	0.391 [9]	0.786 [9]	[35] (exp)
			0.80(4) [9]	
18	-0.129 [9]	0.627 [9]	0.126 [10]	[35] (exp)
			0.130(6) [10]	
30	-0.865 [10]	0.357 [11]	0.714 [11]	[38] (exp)
		0.361(8) [11]	0.70(1) [11]	
35	-0.288 [11]	0.115 [12]	0.231 [12]	[38] (exp)
		0.125(5) [12]	0.235(4) [12]	
39	-0.664 [11]	0.261 [12]	0.521 [12]	[37] (exp)
		0.30(2) [12]	0.56(1) [12]	